

# Approximation schemes for the dynamics of diluted spin models: the Ising ferromagnet on a Bethe lattice

Guilhem Semerjian<sup>1</sup> and Martin Weigt<sup>2</sup>

<sup>1</sup>Laboratoire de Physique Théorique de l'École Normale Supérieure,  
24 rue Lhomond, 75231 Paris Cedex 05, France

<sup>2</sup>Institut für Theoretische Physik, Universität Göttingen,  
Tammannstr. 1, 37077 Göttingen, Germany

guilhem@lpt.ens.fr, weigt@theorie.physik.uni-goettingen.de

October 29, 2018

## Abstract

We discuss analytical approximation schemes for the dynamics of diluted spin models. The original dynamics of the complete set of degrees of freedom is replaced by a hierarchy of equations including an increasing number of global observables, which can be closed approximately at different levels of the hierarchy. We illustrate this method on the simple example of the Ising ferromagnet on a Bethe lattice, investigating the first three possible closures, which are all exact in the long time limit, and which yield more and more accurate predictions for the finite-time behavior. We also investigate the critical region around the phase transition, and the behavior of two-time correlation functions. We finally underline the close relationship between this approach and the dynamical replica theory under the assumption of replica symmetry.

LPT-ENS 04/04

## 1 Introduction

The last few years have seen a considerable increase in the research activity concerning diluted and disordered spin models. This recent interest is mainly driven by two very different, but technically closely related motivations.

The first one aims at understanding common fundamental features of glassy systems, or more generally of out-of-equilibrium problems. Besides various other approaches [1, 2], the study of disordered spin models has led to important insights and given rise to the use of general concepts like, e.g., replica symmetry breaking on the static side [3], or effective temperatures on the dynamic one [4, 5]. Most of these studies were performed on mean-field models, and the validity of these concepts for finite-dimensional systems is still under discussion. For spin models, mean-field has long been another name for fully-connected, i.e. models where each degree of freedom interacts with each other. More recently, a lot of effort was invested in the study of diluted models [6, 7, 8, 9, 10, 11, 12]. These are still mean-field like in the sense that they do not have an underlying geometric structure, and are thus analytically easier to treat than finite-dimensional problems. At the same time, they have finite connectivity: each degree of freedom interacts only with a finite number of neighbors, and the concept of a local environment is well-defined. This allows, e.g., to

introduce microscopically motivated interactions. Diluted models can therefore be considered as an intermediate step between the fully-connected and the finite-dimensional case.

A second major motivation for the study of diluted spin models arises from their close connection with a very interesting class of combinatorial optimization problems [13], including famous problems like satisfiability of Boolean formulas and graph coloring for instance. These problems show phase transitions in the statistical properties of their solutions as well as in the dynamical behavior of algorithms [14, 15, 16], and have thus been extensively studied using tools and concepts originally devised for statistical mechanics purpose [17, 18, 19, 20, 21, 22].

Despite the large interest in diluted models, many basic questions are still open. Whereas the main technical obstacles in analyzing the static behavior are solved by now, and the equilibrium properties of these models are quite well-understood, the knowledge on the dynamical side [23, 24, 25, 26] is still relatively poor. Here we reinvestigate some approximative methods recently introduced for analyzing the behavior of stochastic local search optimization algorithms [27, 28]. We apply and generalize these ideas to a purely physical model, in order to better understand the assumptions behind the approximations made, and to assess their quality. We concentrate on a very simple system, namely a ferromagnetic Ising model defined on a diluted network of fixed connectivity, or Bethe lattice. This example allows to easily present, test and understand approximate methods which should be useful to treat more interesting, glassy problems. In fact the non-equilibrium flavor of this work comes from the study of transient relaxation from an arbitrary initial configuration to thermal equilibrium, and not from the absence of thermal equilibrium as in the case of glassy systems, or from the lack of detailed balance as in previous investigations of algorithms.

The paper is organized as follows. After this general introduction, the model and its equilibrium behavior are presented in Sec. 2. In Sec. 3 the dynamical rules of the model are presented, and a hierarchical approximation scheme is developed. The first three approximations are compared to numerical simulations in Sec. 4, and they are further exploited analytically to describe the critical behavior in Sec. 5. Sec. 6 is dedicated to an extension of the previous approximations to the analysis of two-time quantities. In Sec. 7 we unveil the relation of our approach to the dynamical replica theory proposed by Coolen and Sherrington [29, 30]. Finally, the results are summarized in the last section, and possible future directions of research are presented.

## 2 The model and its equilibrium behavior

We consider a ferromagnetic Ising model on a Bethe lattice, given by its Hamiltonian

$$H = -\frac{1}{2} \sum_{i < j} J_{ij} (\sigma_i \sigma_j - 1) \quad (1)$$

depending on the microscopic configuration  $\vec{\sigma} = (\sigma_1, \dots, \sigma_N)$  of the  $N$  Ising variables  $\sigma_i = \pm 1$ ,  $i = 1, \dots, N$ . The couplings  $J_{ij}$  take the value  $+1$  whenever two spin  $\sigma_i$  and  $\sigma_j$  are connected, and zero otherwise. Compared to the usual form we have shifted the Hamiltonian by its ground state value, and divided it by two. In this way, the Hamiltonian simply counts the *number of unsatisfied edges*, i.e. the number of edges carrying anti-parallel spins on their extremities. It can thus be rewritten as

$$H = \sum_{i < j} J_{ij} \delta_{\sigma_i, -\sigma_j} . \quad (2)$$

The reason why we choose this slightly modified form will become clear below, it allows a simpler presentation of the dynamical equations.

As already said above, we consider this Ising model on a Bethe lattice. In accordance with the recent use in statistical mechanics [7], we define these as random regular graphs, i.e. all vertices have the same degree (number of neighboring sites) [31, 32]. These graphs are locally tree-like. In contrast to Cayley trees they have *no boundary*, all vertices have exactly  $K$  neighbors and are thus equivalent. The graph therefore contains loops for any  $K > 1$ . These are, however, of length  $\mathcal{O}(\ln N)$ , i.e. they become long in the thermodynamic limit  $N \rightarrow \infty$  (with  $K$  kept constant). Note

that the randomness of these graphs appears only through these loops. On finite length scales they appear homogeneous due to their constant vertex degree.

Before investigating the non-equilibrium dynamics of this model, we shortly review its static behavior which can be easily solved using the Bethe-Peierls iterative approach [33, 7]. For doing so, we assume for a moment that our model is defined on a tree, the long loops will be taken into account later as self-consistency conditions.

Consider a given bond  $(i, j)$ , i.e.  $J_{ij} = 1$ . Let us denote  $Z_{i|j}(\sigma_i)$  the partition function of the subtree rooted in  $i$ , with  $(i, j)$  deleted, and with a fixed value of spin  $\sigma_i$ . These partition functions can be easily computed iteratively,

$$Z_{i|j}(\sigma_i) = \prod_{k \neq j | J_{ik}=1} \left( \sum_{\sigma_k = \pm 1} Z_{k|i}(\sigma_k) \exp\{-\beta \delta_{\sigma_i, -\sigma_k}\} \right), \quad (3)$$

where  $\beta$  denotes the inverse temperature. Defining the cavity field

$$h_{i|j} = \frac{1}{2\beta} \ln \left( \frac{Z_{i|j}(+1)}{Z_{i|j}(-1)} \right), \quad (4)$$

we obtain the iterative equations

$$2\beta h_{i|j} = \sum_{k \neq j | J_{ik}=1} \ln \left( \frac{e^{\beta h_{k|i}} + e^{-\beta(1+h_{k|i})}}{e^{\beta(-1+h_{k|i})} + e^{-\beta h_{k|i}}} \right). \quad (5)$$

At this point, we take into account the fact that the model is not defined on a tree, but that all vertices have the same vertex degree and are thus equivalent. We are therefore looking for a self-consistent *homogeneous* solution of Eq. (5) with  $h = h_{i|j}$  for all bonds  $(i, j)$ ,

$$h = \frac{K-1}{2\beta} \ln \left( \frac{e^{\beta h} + e^{-\beta(1+h)}}{e^{\beta(-1+h)} + e^{-\beta h}} \right). \quad (6)$$

This equation has the obvious paramagnetic solution  $h = 0$ . In fact, at high temperature this solution is the only one. There appears, however, a ferromagnetic phase transition at the critical inverse temperature  $\beta_c = \ln(K/(K-2))$ . For lower temperatures, the trivial solution is thermodynamically unstable, and two equivalent ferromagnetic solutions  $\pm h$  describe the equilibrium behavior of the model.

Here and in the following, without any loss of generality, we concentrate only on non-negative  $h$ . Once its value is known, we can immediately compute the Bethe free-energy density (total free-energy divided by  $N$ ),

$$\beta f = (K-1) \ln \left( 2 \cosh \left( \beta \frac{K}{K-1} h \right) \right) - \frac{K}{2} \ln (2 \cosh(2\beta h) + 2e^{-\beta}). \quad (7)$$

Other interesting observables are the energy density

$$e = \frac{\partial \beta f}{\partial \beta} = Kh \tanh \left( \beta \frac{K}{K-1} h \right) - \frac{K}{2} \frac{2h \sinh(2\beta h) - e^{-\beta}}{\cosh(2\beta h) + e^{-\beta}} \quad (8)$$

which equals  $\frac{K}{2}(1 + e^\beta)^{-1}$  in the paramagnetic phase, and the magnetization

$$m = \tanh \left( \beta \frac{K}{K-1} h \right), \quad (9)$$

which becomes positive for positive cavity fields  $h$ . Note that the magnetization  $m$  depends on the cavity field  $h$  via the “true” effective field  $Kh/(K-1)$  which incorporates the contributions of all  $K$  neighbors of a spin, cf. Eqs. (5,6).

To explain some steps of the dynamical approach, we also need the probability  $p_\sigma(u)$  that a randomly selected vertex has spin value  $\sigma$  and belongs to exactly  $u$  unsatisfied edges, i.e.  $u$  out of his  $K$  neighbors have spin  $-\sigma$ . This quantity is given at equilibrium by

$$\begin{aligned} p_+(u) &= \frac{1}{\mathcal{N}_v} \binom{K}{u} e^{-\beta(2h+1)u} , \\ p_-(u) &= \frac{1}{\mathcal{N}_v} \binom{K}{u} e^{-\beta u - 2\beta h(K-u)} , \end{aligned} \quad (10)$$

with  $\mathcal{N}_v$  being a normalization constant enforcing  $\sum_{u,\sigma} p_\sigma(u) = 1$ . This can be rewritten in terms of the energy density and the magnetization as

$$p_\sigma(u) = \frac{1 + \sigma m}{2} \binom{K}{u} \left( \frac{2e}{(1 + \sigma m)K} \right)^u \left( 1 - \frac{2e}{(1 + \sigma m)K} \right)^{K-u} . \quad (11)$$

Similar expressions can be easily derived for the probability  $p_{\sigma_1\sigma_2}(u_1, u_2)$  that a randomly selected edge has a first (resp. second) end vertex of spin  $\sigma_1$  (resp.  $\sigma_2$ ), and this vertex belongs to  $u_1$  (resp.  $u_2$ ) unsatisfied edges,

$$\begin{aligned} p_{++}(u_1, u_2) &= \frac{1}{\mathcal{N}_e} \binom{K-1}{u_1} \binom{K-1}{u_2} e^{-\beta(2h+1)(u_1+u_2)} \\ p_{+-}(u_1, u_2) &= \frac{1}{\mathcal{N}_e} \binom{K-1}{u_1-1} \binom{K-1}{u_2-1} e^{-\beta(u_1+u_2-1) - 2\beta h(u_1-1+K-u_2)} \\ p_{-+}(u_1, u_2) &= \frac{1}{\mathcal{N}_e} \binom{K-1}{u_1-1} \binom{K-1}{u_2-1} e^{-\beta(u_1+u_2-1) - 2\beta h(K-u_1+u_2-1)} \\ p_{--}(u_1, u_2) &= \frac{1}{\mathcal{N}_e} \binom{K-1}{u_1} \binom{K-1}{u_2} e^{-\beta(u_1+u_2) - 2\beta h(2K-u_1-u_2-2)} , \end{aligned} \quad (12)$$

where  $\mathcal{N}_e$  is again determined by normalization.

## 3 Dynamical approximation schemes

### 3.1 Definitions

We will study the following local stochastic dynamics of the model: in each algorithmic step  $T \rightarrow T+1$ , a site  $i$  is chosen at random,  $i \in \{1, \dots, N\}$ . This site is characterized by its spin  $\sigma_i$  and the number  $u_i(\vec{\sigma}) = \sum_j J_{ij} \delta_{\sigma_i, -\sigma_j}$  of its unsatisfied incident edges. The spin is flipped to  $-\sigma_i$  with probability  $W(u_i(\vec{\sigma}), \beta)$ . We denote the new configuration, with spin  $\sigma_i$  flipped, by  $F_i \vec{\sigma}$ .

Obviously all edges incident to site  $i$  which were unsatisfied become satisfied, and vice versa. Hence the variation of the energy if the spin is flipped equals  $\Delta E = K - 2u_i$ . In order to reach thermal equilibrium at inverse temperature  $\beta$  in the long-time limit, we impose the detailed balance condition under the form

$$W(u, \beta) = W(K - u, \beta) \exp(-\beta(K - 2u)) . \quad (13)$$

The two best-known possibilities falling in this category are the Metropolis rate,

$$W(u, \beta) = \min \left( 1, e^{-\beta(K-2u)} \right) , \quad (14)$$

and the Glauber rate,

$$W(u, \beta) = \frac{1}{2} \left( 1 - \tanh \left( \beta \left( \frac{K}{2} - u \right) \right) \right) . \quad (15)$$

We will keep, however, a general form for  $W$  in our analytical treatment, only assuming Eq. (13) to be valid. In the thermodynamic limit, this discrete process acquires a continuous form by

defining the time as  $t = T/N$ , and stepwise differences of extensive observables translate into time derivatives of the corresponding observable densities (extensive observables divided by  $N$ ).

The dynamics of the system, or more precisely of the probabilities  $\mathcal{P}(\vec{\sigma}, t)$  that a microscopic configuration  $\vec{\sigma}$  is found at time  $t$ , can be completely described by the master equation

$$\frac{d}{dt}\mathcal{P}(\vec{\sigma}, t) = \frac{1}{N} \sum_{i=1}^N [-W(u_i(\vec{\sigma}), \beta) \mathcal{P}(\vec{\sigma}, t) + W(u_i(F_i\vec{\sigma}), \beta) \mathcal{P}(F_i\vec{\sigma}, t)] . \quad (16)$$

It is, however, far too complicated to solve these  $2^N$  coupled equations directly. We are therefore going to present several approximative characterizations of the dynamics of the model. They all rely on the same idea: instead of following the evolution of the full distribution  $\mathcal{P}(\vec{\sigma}, t)$  of microscopic configurations, we turn to a simplified description, in terms of a finite number of macroscopic observables. The dynamic evolution of these cannot be expected to be closed, as we have lost information with respect to the microscopic description. It depends in general on a larger number of macroscopic variables, i.e. a hierarchical set of dynamic evolution equations arises. Choosing carefully a closure hypothesis at any level of this hierarchy, we are led to improvingly precise predictions.

In the next three subsections the first three levels of this hierarchy are presented, together with the corresponding closure assumptions. The evaluation of their accuracy is deferred until Sec. 4, where we compare them with numerical simulations.

### 3.2 The binomial approximation

The simplest implementation of this idea consists in keeping track of the energy density  $e(t)$  and of the magnetization per spin  $m(t)$  only.

It is rather natural to include the energy in our set of observables. Indeed, the system is evolving towards equilibrium with respect to the Gibbs measure, in other words, at long times all the microscopic configurations with equilibrium energy are equiprobable. Including the magnetization is also necessary for a ferromagnetic system, where the low temperature phase is characterized by a non zero value of the magnetization. In a more general setting, the minimal set of observables is given by the energy of the system and a complete set of order parameters which allow for the exact description of the equilibrium distribution.

At each time-step, the chosen spin has value  $\sigma$  and  $u$  unsatisfied edges around it with a certain probability  $p_\sigma(u; t)$ . If the flip is accepted, i.e. with probability  $W(u, \beta)$ , the total energy changes by an amount of  $K - 2u$  (unsatisfied edges become satisfied, and *vice versa*), and the variation of the total magnetization is  $-2\sigma$ . We thus obtain in the thermodynamic limit:

$$\frac{de}{dt} = \sum_{u=0}^K W(u, \beta)(K - 2u)[p_-(u; t) + p_+(u; t)] , \quad (17)$$

$$\frac{dm}{dt} = 2 \sum_{u=0}^K W(u, \beta)[p_-(u; t) - p_+(u; t)] . \quad (18)$$

Although exact, these equations are not of direct use because they involve  $p_\sigma(u; t)$ , a dynamical quantity not present in our original description via  $\{e(t), m(t)\}$ . We thus have to express approximately  $p_\sigma(u; t)$  in terms of  $e$  and  $m$  in order to close the set of equations. The randomly selected variable has spin  $\sigma$  with probability  $(1 + \sigma m(t))/2$ . In the absence of further informations, we can only assume that each of the  $K$  incident edges is unsatisfied with the same probability  $\alpha_\sigma(t)$ . This yields the approximate binomial expression

$$p_\sigma(u; t) \simeq \frac{1 + \sigma m(t)}{2} \binom{K}{u} \alpha_\sigma(t)^u (1 - \alpha_\sigma(t))^{K-u} . \quad (19)$$

$\alpha_\pm$  can be determined by the following consistency condition. All unsatisfied edges connect anti-parallel spins. The energy must then be the same if expressed as the number of  $+$  spins around  $-$

spins, or the other way around.

$$\begin{aligned}
e(t) &= \sum_{u=0}^K u p_+(u; t) = \frac{1+m(t)}{2} K \alpha_+(t) \\
&= \sum_{u=0}^K u p_-(u; t) = \frac{1-m(t)}{2} K \alpha_-(t) .
\end{aligned} \tag{20}$$

We finally obtain

$$p_\sigma(u; t) = \frac{1 + \sigma m(t)}{2} \binom{K}{u} \left( \frac{2e(t)}{K(1 + \sigma m(t))} \right)^u \left( 1 - \frac{2e(t)}{K(1 + \sigma m(t))} \right)^{K-u} . \tag{21}$$

This expression has the same form as the equilibrium equation (11), but with  $e(t)$  and  $m(t)$  being dynamical variables, which can differ from their equilibrium values.

Equations (17), (18) and (21) can be condensed into

$$\frac{de}{dt} \equiv F_e(e(t), m(t), \beta) , \tag{22}$$

$$\frac{dm}{dt} \equiv F_m(e(t), m(t), \beta) . \tag{23}$$

A few expected properties of these equations can be checked immediately:

- $F_m(e, m = 0, \beta) = 0$  for all  $e$  and  $\beta$ . If the system is strictly unmagnetized, the dynamics does not break this symmetry in the thermodynamic limit. In the low temperature phase, there is of course an instability with respect to magnetization fluctuations (which are present in any finite system), as we shall show in Sec. 5.
- $F_e(e_p, m = 0, \beta) = 0$  where  $e_p = \frac{K}{2}(1 + e^\beta)^{-1}$  is the paramagnetic energy density at inverse temperature  $\beta$ . To prove this, one can note that in that case

$$p_+(K - u) = e^{-\beta(K-2u)} p_-(u) . \tag{24}$$

Using the detailed balance condition on  $W$  and the change of variables  $u \mapsto K - u$  in one of the sums defining  $F_e$ , one thus shows that the paramagnetic state is a fixed point of the dynamics.

- $F_e(e_f, m_f, \beta) = F_m(e_f, m_f, \beta) = 0$  for  $\beta > \beta_c$ , where  $m_f$  and  $e_f$  are the magnetization and the energy density of the ferromagnetic phase. Indeed, relation (24) is still valid, as can be seen from (10), and the proof follows the same line as in the paramagnetic case: the ferromagnetic state, when present, is also a fixed point of the dynamics.

### 3.3 Independent-neighbor approximation

In the last section, we have described the dynamics of our ferromagnetic model by mapping it to two coupled differential equations for the energy and the magnetization. In order to approximately close these equations we had to assume a specific binomial form for the quantities  $p_\sigma(u; t)$  which is exactly valid only in thermal equilibrium, but not for intermediate times. It seems therefore natural to extend the set of considered observables, and to look for dynamical equations for  $p_\sigma(u; t)$  itself. Note that on regular graphs, these quantities still form a finite set of observables. This would not be the case for a graph with unbounded fluctuations of the connectivities.

To formulate the dynamical equations, we have to take into account different contributions to the variation of  $p_\sigma(u; t)$  during a time-step:

- The first type of contribution is due to the flipped spin itself, i.e.  $\sigma$  is flipped to  $-\sigma$ . All incident edges change from satisfied to unsatisfied and vice versa, i.e. we have  $u \leftrightarrow K - u$ .

- The second type comes from the neighbors of the flipped spin. For these vertices,  $\sigma$  remains obviously unchanged, but  $u$  is increased or decreased by one depending on whether the connecting edge was satisfied or not before the flip.

Including the corresponding loss and gain terms, we find the following exact equations,

$$\begin{aligned}
\frac{d}{dt} p_\sigma(u; t) &= -W(u, \beta) p_\sigma(u; t) + W(K - u, \beta) p_{-\sigma}(K - u; t) \\
&+ \sum_{\tilde{u}} (K - \tilde{u}) W(\tilde{u}, \beta) p_\sigma(\tilde{u}; t) [-p(u|\sigma, \tilde{u} \rightarrow \sigma; t) + p(u - 1|\sigma, \tilde{u} \rightarrow \sigma; t)] \\
&+ \sum_{\tilde{u}} \tilde{u} W(\tilde{u}, \beta) p_{-\sigma}(\tilde{u}; t) [-p(u|-\sigma, \tilde{u} \rightarrow \sigma; t) + p(u + 1|-\sigma, \tilde{u} \rightarrow \sigma; t)] \quad (25)
\end{aligned}$$

where  $p(u|\tilde{\sigma}, \tilde{u} \rightarrow \sigma; t)$  is the conditional probability that a vertex of spin  $\sigma$  belongs exactly to  $u$  unsatisfied edges, under the condition that this vertex is reached via an edge coming from a vertex with spin  $\tilde{\sigma}$  and with  $\tilde{u}$  unsatisfied bonds. This probability can be computed from the joint probability  $p_{\tilde{\sigma}\sigma}(\tilde{u}, u; t)$  of two adjacent vertices which, in the equilibrium context, was already introduced at the end of Sec. 2:

$$p(u|\tilde{\sigma}, \tilde{u} \rightarrow \sigma; t) = \frac{p_{\tilde{\sigma}\sigma}(\tilde{u}, u; t)}{\sum_{\tilde{u}} p_{\tilde{\sigma}\sigma}(\tilde{u}, u; t)}. \quad (26)$$

As in the previous subsection, these exact equations do not close. The time evolution of the probabilities  $p_\sigma(u; t)$  is given in terms of the correlations between neighboring vertices,  $p_{\tilde{\sigma}\sigma}(\tilde{u}, u; t)$ . We can, however, close the equations at least approximately by considering neighbors as independent [28],

$$\begin{aligned}
p(u|\sigma, \tilde{u} \rightarrow \sigma; t) &\simeq \frac{(K - u) p_\sigma(u; t)}{\langle K - u \rangle_\sigma} \\
p(u|-\sigma, \tilde{u} \rightarrow \sigma; t) &\simeq \frac{u p_\sigma(u; t)}{\langle u \rangle_\sigma}, \quad (27)
\end{aligned}$$

i.e. the conditional probability does not depend on the properties of the initial vertex, but only on the fact that we reach the new vertex via a satisfied or an unsatisfied edge. In the last equation we have used the short-hand notation  $\langle \bullet \rangle_\sigma = \sum_u \bullet p_\sigma(u; t)$ . Note that this does not describe an average since, for instance,  $\langle 1 \rangle_\sigma$  equals the fraction of spins with value  $\sigma$ , and normalization holds only for  $\langle \bullet \rangle_+ + \langle \bullet \rangle_-$ .

Under this approximation, Eq. (25) closes in  $p_\sigma(u; t)$  and becomes

$$\begin{aligned}
\frac{d}{dt} p_\sigma(u; t) &= -W(u, \beta) p_\sigma(u; t) + W(K - u, \beta) p_{-\sigma}(K - u; t) \\
&+ \frac{\langle (K - \tilde{u}) W(\tilde{u}, \beta) \rangle_\sigma}{\langle K - \tilde{u} \rangle_\sigma} [-(K - u) p_\sigma(u; t) + (K - u + 1) p_\sigma(u - 1; t)] \\
&+ \frac{\langle \tilde{u} W(\tilde{u}, \beta) \rangle_{-\sigma}}{\langle \tilde{u} \rangle_\sigma} [-u p_\sigma(u; t) + (u + 1) p_\sigma(u + 1; t)] \quad (28)
\end{aligned}$$

An important observation is that Eq. (27) becomes exact for the equilibrium distributions (10) and (12). Therefore the true thermal equilibrium is a fixed point of the closed dynamical equations. For intermediate times, however, there will be deviations from Eq. (28). Since the description via  $p_\sigma(u; t)$  is, however, more detailed than the one of the binomial approximation, we expect deviations to be less important. A thorough comparison with Monte-Carlo simulations will be given in Sec. 4.

These equations are ordinary differential equations and can thus be solved numerically by standard methods. One has, however, to be careful with the choice of initial conditions. In fact, not every normalized  $p_\sigma(u)$  corresponds to microscopic configurations  $(\sigma_1, \dots, \sigma_N)$ . A necessary

and sufficient consistency condition is given by the fact that each unsatisfied edge connects two antiparallel spins, see the discussion before Eq. (20). Therefore

$$\sum_u u p_+(u; t) = \sum_u u p_-(u; t) \quad (29)$$

must hold for arbitrary time  $t$ . Restricting the allowed initial conditions to all  $p_\sigma(u; t)$  fulfilling this condition, consistency is preserved by the dynamical evolution (28). This in fact guarantees that the only stationary points of the dynamics are the solutions of the equilibrium study of Sec. 2. In the high-temperature phase, the paramagnetic solution attracts the dynamics, while the low-temperature phase allows for three stationary points. The two ferromagnetic ones are stable, whereas the paramagnetic solution is unstable with respect to any spin-flip asymmetry ( $p_\sigma(u; t_0) \neq p_{-\sigma}(u; t_0)$ ) in the initial condition.

### 3.4 Inclusion of neighbor correlations

In order to further refine the description of the non-equilibrium behavior of the model, we may “iterate” the step which led us from the binomial to the independent-neighbor approximation. The exact equations for the evolution of the single-site quantity  $p_\sigma(u; t)$  depend on the joint distribution  $p_{\bar{\sigma}\sigma}(\bar{u}, u; t)$  for neighboring sites. Formulating an equation for the time evolution of the latter quantity, which again includes a finite set of functions, we find an equation including three-spin correlations. Approximately, these can be expressed in terms of the two-spin distribution, and the dynamical equations close. In the formulation of the equations we have to include the effects of the flipped spin itself, and of its first and second neighbors. We only give the resulting equations, where the time dependence is not stated explicitly to lighten notations:

$$\begin{aligned} \frac{d}{dt} p_{\sigma\sigma}(u_1, u_2) &= -W(u_1, \beta) p_{\sigma\sigma}(u_1, u_2) + W(K - u_1, \beta) p_{-\sigma\sigma}(K - u_1, u_2 + 1) \\ &+ \sum_u W(u, \beta) [ -p_{\sigma\sigma}(u, u_1) (K - u_1 - 1) p(u_2|\sigma, u_1 \rightarrow \sigma) \\ &\quad + p_{\sigma\sigma}(u, u_1 - 1) (K - u_1) p(u_2|\sigma, u_1 - 1 \rightarrow \sigma) \\ &\quad - p_{-\sigma\sigma}(u, u_1) (K - u_1) p(u_2|\sigma, u_1 \rightarrow \sigma) \\ &\quad + p_{-\sigma\sigma}(u, u_1 + 1) (K - u_1 - 1) p(u_2|\sigma, u_1 + 1 \rightarrow \sigma) ] \\ &+ (u_1 \leftrightarrow u_2) , \\ \frac{d}{dt} p_{-\sigma\sigma}(u_1, u_2) &= -[W(u_1, \beta) + W(u_2, \beta)] p_{-\sigma\sigma}(u_1, u_2) \\ &+ W(K - u_1, \beta) p_{\sigma\sigma}(K - u_1, u_2 - 1) + W(K - u_2, \beta) p_{-\sigma-\sigma}(u_1 - 1, K - u_2) \\ &+ \sum_u W(u, \beta) [ -p_{\sigma-\sigma}(u, u_1) (u_1 - 1) p(u_2|-\sigma, u_1 \rightarrow \sigma) \\ &\quad + p_{\sigma-\sigma}(u, u_1 + 1) u_1 p(u_2|-\sigma, u_1 + 1 \rightarrow \sigma) \\ &\quad - p_{-\sigma-\sigma}(u, u_1) u_1 p(u_2|-\sigma, u_1 \rightarrow \sigma) \\ &\quad + p_{-\sigma-\sigma}(u, u_1 - 1) (u_1 - 1) p(u_2|-\sigma, u_1 - 1 \rightarrow \sigma) \\ &\quad - p_{\sigma\sigma}(u, u_2) u_2 p(u_1|\sigma, u_2 \rightarrow -\sigma) \\ &\quad + p_{\sigma\sigma}(u, u_2 - 1) (u_2 - 1) p(u_1|\sigma, u_2 - 1 \rightarrow -\sigma) \\ &\quad - p_{-\sigma\sigma}(u, u_2) (u_2 - 1) p(u_1|\sigma, u_2 \rightarrow -\sigma) \\ &\quad + p_{-\sigma\sigma}(u, u_2 + 1) u_2 p(u_1|\sigma, u_2 + 1 \rightarrow -\sigma) ] , \end{aligned} \quad (30)$$

where  $(u_1 \leftrightarrow u_2)$  means that the complete expression on the right-hand side of the equation with  $u_1$  and  $u_2$  interchanged has to be added. In the following, these equations will be denoted shortly as *link approximation*. As in the case of the single-site quantities, they have to be solved numerically. The  $p_\sigma(u)$  can be recovered from the pair distribution in two distinct ways:

$$\sum_{u_2} p_{\sigma\sigma}(u_1, u_2) \propto (K - u_1) p_\sigma(u_1) \quad (31)$$

and

$$\sum_{u_2} p_{\sigma-\sigma}(u_1, u_2) \propto u_1 p_{\sigma}(u_1). \quad (32)$$

These two procedures must yield the same value of  $p_{\sigma}(u)$ . This consistency condition ensures, in analogy to Eq. (29) for the previous approximation scheme, that the only stationary points are those given by the static approach.

In principle, one could go on like this, i.e. equations for higher-order correlations can be written down exactly. They will depend on even higher correlations, and an infinite hierarchy of exact equations arises. This hierarchy can be cut approximately at any arbitrary level by factorizing higher correlations. Since the number of order parameters used to describe the dynamics increases with each level, and the observables of lower levels are contained via consistency conditions, the description is expected to become more and more precise. On the other hand, the equations become more and more complex, as is already clear when one compares them for the three first levels of the approximation hierarchy. Instead of continuing further in this way, we compare now the results of the first three approximation levels with Monte Carlo simulations. As we shall see, already these approximations give an astonishing coincidence with numerical data.

## 4 Comparison with numerics

The approximation schemes presented in the last section do not possess any intrinsic criterion to measure their quality. We therefore have performed numerical simulations for large graphs in order to check all three schemes.

To do so, we have first generated large random regular graphs ( $N = 3 \cdot 10^6$ ) of various connectivities, according to the algorithm of [32]. Then we have performed Monte Carlo simulations of the ferromagnetic Ising model defined on this graph. In these simulations, we have used as well Glauber as Metropolis dynamics, cf. Sec. 3.1. In the following presentation we concentrate, however, solely on the Metropolis case. The results for Glauber dynamics differ quantitatively, but the coincidence between numerical and analytical results has the same quality. To suppress finite-size fluctuations, which become important for large times close to the critical point, we have averaged numerical data for up to 200 independent runs on independently generated graphs.

In general, we have initialized the system in the following way: all spins are assigned randomly and independently a value, with a certain bias in order to impose some initial magnetization on the system. Note that this configuration is not an equilibrium configuration for any arbitrary temperature. Then we have measured the relaxational dynamics from this non-equilibrium configuration to thermal equilibrium, and recorded in particular the time evolution of the energy density  $e(t)$  and of the global magnetization  $m(t)$ .

As a result, as represented in Figs. 1 and 2, we have found the following behavior: for very short and very long time, all three approximation schemes are in extremely good coincidence with numerical data. This is even true close to the critical temperature, all three schemes reproduce with high precision the critical slowing down, i.e. the diverging longest time scale in the system. Exactly at the critical point, all three approximation schemes show the correct algebraic relaxation towards equilibrium. So even the simplest approximation, which can be analyzed in large detail, see the next section, allows for a precise estimate of the relaxational dynamics close to equilibrium.

As shown in the insets of Figs. 1 and 2, considerable deviations between numerical data and analytical predictions appear only for intermediate times. As to be expected, these deviations become smaller for more detailed approximations. In the link-approximation, these deviations are hardly visible for all times, even at the critical point.

In addition, we have observed an increasing precision of all three approximations for growing  $K$ . We expect therefore, that the binomial approximation becomes exact in the large- $K$  limit [27].

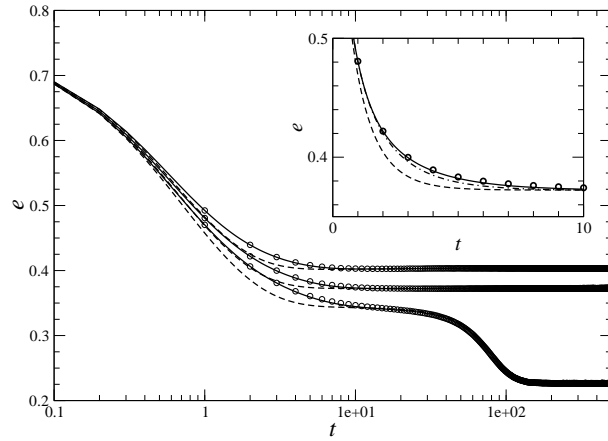


Figure 1: Energy density as a function of time. The three approximations (dashed line = binomial, dash-dotted = independent neighbor, full = link approximation) are compared to numerical simulations (symbols,  $N = 3 \cdot 10^6$ ,  $K = 3$ , averaged over 200 runs, error bars are smaller than the symbol size) for inverse temperatures  $\beta = 1.0, \ln 3, 1.2$  (top to bottom), with critical value  $\beta_c = \ln 3$ . In the initial condition all spins were drawn independently, with average magnetization 0.1. In the main plot, the independent neighbor approximation is not shown because, on the scale of the figure, it is very close to the link approximation. The shoulder in the curve for  $\beta = 1.2$  is located close to the paramagnetic energy value, the relaxation to the ferromagnetic state appears on a longer time scale. The inset enlarges the region of largest deviation between the different approximations for  $\beta_c$ . Obviously, the more involved schemes lead to better approximations, the difference between the link approximation and the numerical data is hardly visible.

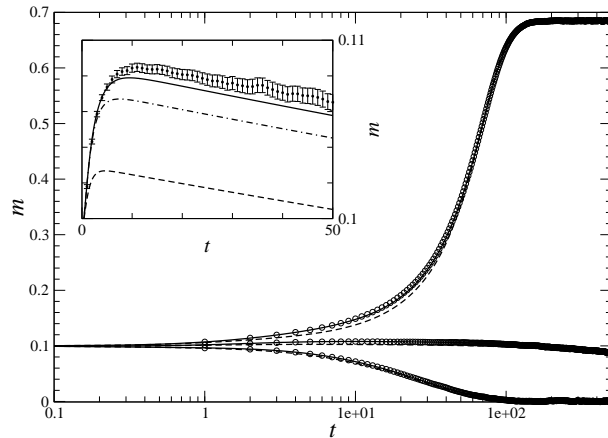


Figure 2: Magnetization as a function of time. The parameters and symbols are the same as in Fig. 1. Again, the coincidence of the link approximation with the numerical data is excellent for the full time interval.

## 5 Critical behavior

In this section we investigate in more detail the predictions of our approximations in the critical region of temperatures separating the paramagnetic and the ferromagnetic phase. For the sake of simplicity, we concentrate on the first two levels of approximations, for which more detailed computations can be done explicitly.

As we have seen before, all the presented dynamical approximations have fixed points corresponding to paramagnetic and ferromagnetic equilibrium. One has to study now the nature of the dynamical flows in the space of projected order parameters. At high temperatures, the only fixed point is the paramagnetic one, and it is obvious on physical grounds that it will be stable. In the low temperature phase, this fixed point will become unstable and the two ferromagnetic ones will attract the dynamics.

Quite generally, if the projected evolution is described by an  $n$ -component vector  $\vec{q}(t)$  of observables, the system's evolution is given by  $n$  equations  $\dot{q}_i = F_i(\vec{q})$ . Fixed points correspond to  $F_i(\vec{q}_0) = 0 \forall i$ . They are locally stable if and only if all eigenvalues of the  $n \times n$  matrix  $\mathcal{M}$  are negative, where  $\mathcal{M}$  is defined by its entries  $\mathcal{M}_{ij} = (\partial F_i)/(\partial q_j)$ , evaluated at the fixed point under consideration. In this case, the asymptotic relaxation of a fluctuation towards equilibrium is given by the largest eigenvalue  $\lambda_{max}$  (smallest in absolute value), and the longest relaxation-time scale of the model reads

$$\tau = -(\lambda_{max})^{-1}. \quad (33)$$

Approaching the critical point, this eigenvalue tends to zero. The system slows down until the relaxation time eventually diverges at  $\beta_c$ . Right at the critical point, fluctuations decay only algebraically with time.

### 5.1 Relaxation time and critical slowing down in the binomial approximation

In the simplest case of the binomial approximation, the space of parameters is only two-dimensional, the state of the system being characterized by its magnetization and energy. Following the notations of Sec. 3.2, we define the matrix  $\mathcal{M}$  by

$$\mathcal{M} = \begin{pmatrix} \mathcal{M}_{ee} & \mathcal{M}_{em} \\ \mathcal{M}_{me} & \mathcal{M}_{mm} \end{pmatrix} = \begin{pmatrix} \frac{\partial F_e}{\partial e} & \frac{\partial F_e}{\partial m} \\ \frac{\partial F_m}{\partial e} & \frac{\partial F_m}{\partial m} \end{pmatrix}. \quad (34)$$

This matrix takes a particularly simple form when computed at the paramagnetic fixed point. Indeed, the symmetry of the system under magnetization reversal causes the non-diagonal elements to vanish, and one can directly read the eigenvalues of  $\mathcal{M}$  in the diagonal entries,

$$\mathcal{M}_{ee} = -\frac{1}{K} \frac{1 + e^\beta}{(1 + e^{-\beta})^{K-1}} \sum_{u=0}^K \binom{K}{u} W(u, \beta) e^{-\beta u} (K - 2u)^2, \quad (35)$$

$$\mathcal{M}_{mm} = -\frac{2 - K + K e^{-\beta}}{(1 + e^{-\beta})^K} \sum_{u=0}^K \binom{K}{u} W(u, \beta) e^{-\beta u}. \quad (36)$$

It is obvious from these expressions that  $\mathcal{M}_{ee}$  is negative at all temperatures, and that  $\mathcal{M}_{mm}$  changes its sign at the critical temperature  $\beta_c = \ln(K/(K - 2))$ . At low temperature, the paramagnetic fixed point becomes unstable against fluctuations of the magnetization, as expected on physical grounds.

From the above expression of  $\mathcal{M}_{mm}$  one obtains the divergence of the relaxation time of the system when approaching the critical temperature from above,

$$\tau_p \underset{\beta \rightarrow \beta_c^-}{\sim} (\beta_c - \beta)^{-1} \left[ \frac{K - 2}{(1 + e^{-\beta_c})^K} \sum_{u=0}^K \binom{K}{u} W(u, \beta_c) e^{-\beta_c u} \right]^{-1}. \quad (37)$$

In the low temperature phase, at the ferromagnetic fixed point (we consider only the one with positive magnetization for simplicity), the four elements are different from zero. Both eigenvalues of  $\mathcal{M}$  are negative, implying the stability of the ferromagnetic phase. As their expressions at general temperature is not very illuminating, we concentrate on the  $\beta \rightarrow \beta_c^+$  limit, for which one finds the following scaling of the matrix elements:

$$\mathcal{M}_{ee} \rightarrow a < 0 \quad , \quad \mathcal{M}_{em} \sim b\sqrt{\beta - \beta_c} \quad , \quad \mathcal{M}_{me} \sim c\sqrt{\beta - \beta_c} \quad , \quad \mathcal{M}_{mm} \sim d(\beta - \beta_c) \quad , \quad (38)$$

where  $a$ ,  $b$ ,  $c$  and  $d$  can be explicitly computed in terms of  $W(u, \beta_c)$ . This implies that the relevant eigenvalue vanishes as

$$\lambda \sim \left( d - \frac{bc}{a} \right) (\beta - \beta_c) \quad . \quad (39)$$

After some algebra to simplify the expression, we obtain finally the divergence of the relaxation time from the ferromagnetic side of the transition as

$$\tau_f \underset{\beta \rightarrow \beta_c^+}{\sim} (\beta - \beta_c)^{-1} \left[ \frac{2(K-2)}{(1+e^{-\beta_c})^K} \sum_{u=0}^K \binom{K}{u} W(u, \beta_c) e^{-\beta_c u} \right]^{-1} \quad . \quad (40)$$

The two expressions (37) and (40) show an universal amplitude ratio of 1/2.

## 5.2 Relaxation time and critical slowing down in the independent-neighbor approximation

The analysis becomes more involved in the independent-neighbor approximation. As said above, we have to compute the  $2(K+1) \times 2(K+1)$  matrix

$$\mathcal{M} = \begin{pmatrix} \partial \dot{p}_{\sigma_1}(u_1; t) \\ \partial p_{\sigma_2}(u_2; t) \end{pmatrix} \quad (41)$$

starting from equation (28), evaluated at the equilibrium distribution  $p_{\sigma_2}(u_2)$  given in (10). The matrix elements are thus given by

$$\begin{aligned} \mathcal{M}_{\sigma, \sigma}(u_1, u_2) &= -W(u_1, \beta) \delta_{u_1, u_2} \\ &+ \frac{\langle (K-u)W(u, \beta) \rangle_{\sigma}}{\langle K-u \rangle_{\sigma}} [- (K-u_1) \delta_{u_1, u_2} + (K-u_1+1) \delta_{u_1-1, u_2}] \\ &+ [-(K-u_1)p_{\sigma}(u_1) + (K-u_1+1)p_{\sigma}(u_1-1)] \\ &\quad \times \left[ \frac{(K-u_2)W(u_2, \beta)}{\langle K-u \rangle_{\sigma}} - \frac{\langle (K-u)W(u, \beta) \rangle_{\sigma} (K-u_2)}{\langle K-u \rangle_{\sigma}^2} \right] \\ &+ \frac{\langle uW(u, \beta) \rangle_{-\sigma}}{\langle u \rangle_{\sigma}} [-u_1 \delta_{u_1, u_2} + (u_1+1) \delta_{u_1+1, u_2}] \\ &+ [-u_1 p_{\sigma}(u_1) + (u_1+1)p_{\sigma}(u_1+1)] \frac{\langle uW(u, \beta) \rangle_{-\sigma} u_2}{\langle u \rangle_{\sigma}^2} \quad , \\ \mathcal{M}_{\sigma, -\sigma}(u_1, u_2) &= W(K-u_1, \beta) \delta_{K-u_1, u_2} \\ &+ \frac{u_2 W(u_2, \beta)}{\langle u \rangle_{\sigma}} [-u_1 p_{\sigma}(u_1) + (u_1+1)p_{\sigma}(u_1+1)] \quad . \end{aligned} \quad (42)$$

The relaxation times equal minus the inverse eigenvalues of this matrix. One has, however, to be careful since not all eigenvectors correspond to physically allowed deviations of  $p_{\sigma}(u; t)$  from its equilibrium value. As already discussed in Sec. 3.3, the values of  $p_{\sigma}(u)$  are restricted by normalization and by the consistency condition (29). The corresponding eigenvectors, one being proportional to  $p_{\sigma}(u)$  itself, the other one to the deviation  $\partial p_{\sigma}(u)/\partial h$  according to a deviation of

the effective field  $h$  away from its self-consistent cavity value, correspond to zero eigenvalues of  $\mathcal{M}$ , and have to be excluded.

The most efficient way to achieve this is to explicitly require normalization and consistency by, e.g., expressing  $p_{\pm}(K; t)$  through the other values  $p_{\pm}(u; t)$  with  $u < K$ . From normalization and consistency we immediately find

$$p_{\sigma}(K; t) = \frac{1}{2} \left[ 1 - \sum_{u=0}^{K-1} \left( \frac{K+u}{K} p_{\sigma}(u; t) + \frac{K-u}{K} p_{-\sigma}(u; t) \right) \right]. \quad (43)$$

The matrix  $\mathcal{M}$  becomes thereby reduced to a  $2K$ -dimensional matrix  $\tilde{\mathcal{M}}$  with entries ( $u_{1,2} = 0, \dots, K-1$ )

$$\begin{aligned} \tilde{\mathcal{M}}_{\sigma_1, \sigma_2}(u_1, u_2) &= \frac{\partial p_{\sigma_1}(u_1; t)}{\partial p_{\sigma_2}(u_2; t)} + \sum_{\sigma=\pm 1} \frac{\partial p_{\sigma_1}(u_1; t)}{\partial p_{\sigma}(K; t)} \frac{\partial p_{\sigma}(K; t)}{\partial p_{\sigma_2}(u_2; t)} \\ &= \mathcal{M}_{\sigma_1, \sigma_2}(u_1, u_2) - \sum_{\sigma=\pm 1} \frac{K - u\sigma_1\sigma}{2K} \mathcal{M}_{\sigma_1, \sigma}(u_1, K). \end{aligned} \quad (44)$$

Besides the excluded unphysical eigenvectors, this matrix has the same eigenvalues and eigenvectors as  $\mathcal{M}$ .

Unfortunately, we were not able to find a general expression for the smallest eigenvalue of  $\tilde{\mathcal{M}}$  for arbitrary temperature, and thus of the longest relaxation time of the system. For small values of  $K$ , the latter can, however, easily be evaluated using a standard computer-algebra system. We find, in complete accordance with the binomial approximation, that the longest relaxation time scale diverges like  $\tau_p = A_K(\beta_c - \beta)^{-1}$  if the critical point is reached from the paramagnetic side, and like  $\tau_f = \frac{1}{2}A_K(\beta - \beta_c)^{-1}$  coming from lower temperature. We thus find the same critical exponent and the same universal amplitude ratio 1/2. Only the prefactors are slightly modified, with a difference of about 1-2% only between the estimates of the binomial and of the independent-neighbor approximations. The values for Metropolis dynamics are recorded in the table below.

$K$	$A_K$ (binomial)	$A_K$ (independent neighbor)
3	$\frac{16}{5} = 3.2$	$\frac{1882}{557} \simeq 3.273043$
4	$\frac{27}{28} \simeq 0.964286$	$\frac{1146337}{1162000} \simeq 0.986521$
5	0.605604	0.609906
6	0.393775	0.398242
7	0.309897	0.311649

In Fig. 3, the results of both approximations are compared to numerical data. The results of the independent neighbor approximation are slightly higher than the binomial ones. In perfect agreement with this observation, also the numerical data are found to systematically deviate towards slightly higher relaxation times. Note, however, that the extraction of the relaxation time in the ferromagnetic phase is slightly subtle: the time interval between the pre-asymptotic and the fluctuation-dominated dynamics is rather short even for large systems ( $N = 3 \cdot 10^6$ , averaged over 20 samples).

### 5.3 Algebraic relaxation at criticality

At the critical point  $\beta_c$ , the longest time scale diverges, and the observables of the system decay only algebraically towards their equilibrium values. Within the binomial approximation, the dynamical exponents for energy and magnetization decay as well as their prefactors can be determined analytically.

The equilibrium at the critical point is given by a non-magnetized state of energy density  $e_c = \frac{K(K-2)}{4(K-1)}$ . If the initial condition has vanishing magnetization, the energy relaxes exponentially

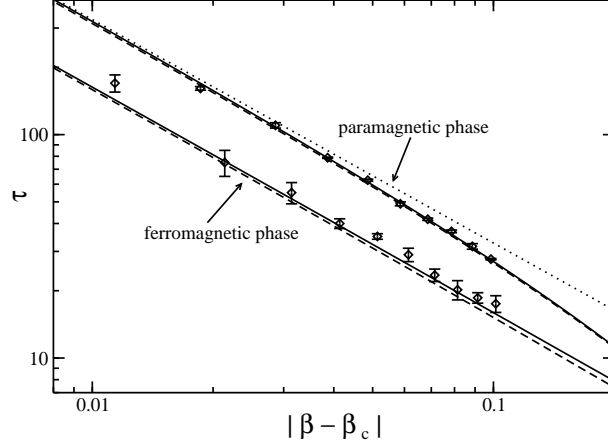


Figure 3: Metropolis relaxation time for  $K = 3$  in the paramagnetic (top) and the ferromagnetic (bottom) phase. We have plotted the results of the binomial (dashed line) and the independent-neighbor (full line) approximations as extracted from the exact eigenvalues of the matrices  $\mathcal{M}$ . The dotted line gives the asymptotic algebraic divergence in the paramagnetic phase. The symbols are extracted from numerical simulations ( $N = 3 \cdot 10^6$ , 20 samples).

towards  $e_c$ . However, if the evolution starts from an initial condition of arbitrarily small, but non-zero magnetization, the dynamical evolution shows a power-law dependence in time.

Let us denote the excess-energy density by  $\hat{e} = e - e_c$ , and expand the evolution equations around their fixed point ( $e_c, m = 0$ ). Exploiting the spin-flip symmetry  $m \leftrightarrow -m$  and the fact that  $\partial_m F_m$  vanishes at the critical temperature, we obtain for the lowest orders

$$\frac{d\hat{e}}{dt} = C_{10}^{(e)} \hat{e} + C_{02}^{(e)} m^2 + C_{20}^{(e)} \hat{e}^2 + C_{12}^{(e)} \hat{e} m^2 + \dots, \quad (45)$$

$$\frac{dm}{dt} = C_{11}^{(m)} \hat{e} m + C_{03}^{(m)} m^3 + C_{21}^{(m)} \hat{e}^2 m + C_{13}^{(m)} \hat{e} m^3 + C_{05}^{(m)} m^5 + \dots, \quad (46)$$

where the coefficients are given by

$$C_{ij}^{(m/e)} = \frac{1}{i! j!} \left. \frac{\partial^{i+j} F_{m/e}(e, m, \beta_c)}{\partial^i e \partial^j m} \right|_{e=e_c, m=0}. \quad (47)$$

To extract the leading algebraic long-time behavior

$$m(t) \sim m_0 t^{-z_m}, \quad \hat{e} \sim \hat{e}_0 t^{-z_e}, \quad (48)$$

we have to compare the dominant terms on both sides of the equations. Seen that the lhs of the first equation is of  $\mathcal{O}(t^{-z_e-1})$ , the asymptotically larger  $\mathcal{O}(t^{-z_e})$ -term on the rhs has to be compensated by the second contribution with  $\mathcal{O}(t^{-2z_m})$ . This results in  $z_e = 2z_m$ . The lhs of the second equation is of  $\mathcal{O}(t^{-z_m-1})$ , whereas the two dominant terms on its rhs are of  $\mathcal{O}(t^{-z_e-z_m}) = \mathcal{O}(t^{-3z_m})$ . Comparing the order of these terms we consequently find

$$z_m = \frac{1}{2}, \quad z_e = 1. \quad (49)$$

These exponents stand in perfect agreement with numerical simulations. Considering in addition the coefficients of the discussed contributions, we are led to

$$0 = \hat{e}_0 \frac{\partial F_e}{\partial e} + \frac{1}{2} m_0^2 \frac{\partial^2 F_e}{\partial m^2}, \quad (50)$$

$$-\frac{1}{2} m_0 = \hat{e}_0 m_0 \frac{\partial^2 F_m}{\partial e \partial m} + \frac{1}{6} m_0^3 \frac{\partial^3 F_m}{\partial m^3}, \quad (51)$$

where the derivatives have to be evaluated at the fixed point  $(e_c, m = 0)$ . After some algebra, we obtain the prefactors of magnetization and excess energy:

$$m_0^2 = \frac{3K}{2(K-2)} \left( \frac{2(K-1)}{K} \right)^{K-1} \left[ \sum_{u=0}^K \binom{K}{u} W(u, \beta_c) e^{-\beta_c u} \right]^{-1}, \quad (52)$$

$$\hat{e}_0 = -\frac{K-2}{4} m_0^2. \quad (53)$$

Note that there are two solutions  $m_0 = \pm \sqrt{m_0^2}$ , depending of the sign of the magnetization in the initial condition. The quality of the agreement between these predictions and numerical simulations (not shown) is comparable to the one of previous subsection.

## 6 Two-time correlations

We briefly sketch in this section an extension of the previously introduced approximations to the study of two-time quantities, more precisely of the global auto-correlation function of the spins,

$$C(t_2, t_1) = \frac{1}{N} \sum_{i=1}^N \sigma_i(t_2) \sigma_i(t_1). \quad (54)$$

These will be, in the thermodynamic limit, sharply peaked around its average value (with respect to the possible histories of the microscopic dynamics). We suppose in the following  $t_2 \geq t_1$  to simplify the notations. To compute this function, we shall consider  $t_2$  as the evolution time and project the dynamics onto a global observable which retains a trace of the microscopic configuration at the earlier time  $t_1$ . More precisely, let us call  $q_{\sigma_1 \sigma_2}(uu, us, su; t_1, t_2)$  the fractions of sites whose spin equals  $\sigma_1$  at time  $t_1$  and  $\sigma_2$  at time  $t_2$ , and which have around them

- $uu$  edges which are unsatisfied at both times,
- $us$  which are unsatisfied at time  $t_1$  and satisfied at time  $t_2$ ,
- $su$  which are satisfied at time  $t_1$  and unsatisfied at time  $t_2$ ,
- and  $ss \equiv K - uu - us - su$  which are satisfied at both times.

We introduce the notation

$$\langle \bullet \rangle_{\sigma_1 \sigma_2} = \sum_{\substack{uu, us, su \\ uu + us + su \leq K}} \bullet \cdot q_{\sigma_1 \sigma_2}(uu, us, su; t_1, t_2), \quad (55)$$

which is again not a normalized average for a given value of  $\sigma_1$  and  $\sigma_2$ , but only when the sum is taken over all indices,  $\langle 1 \rangle_{++} + \langle 1 \rangle_{+-} + \langle 1 \rangle_{-+} + \langle 1 \rangle_{--} = 1$ . The two-time correlation of the spins can be obtained from  $q$ , and reads in this short-hand notation:

$$C(t_2, t_1) = \langle 1 \rangle_{++} + \langle 1 \rangle_{--} - \langle 1 \rangle_{+-} - \langle 1 \rangle_{-+}. \quad (56)$$

As in the previous cases, one has to impose consistency equations on  $q$ , to ensure that the number of unsatisfied edges around up or down spins is the same. Enforcing this condition at  $t_1$  and  $t_2$  yields respectively:

$$\langle uu + us \rangle_{++} + \langle uu + us \rangle_{+-} = \langle uu + us \rangle_{-+} + \langle uu + us \rangle_{--}. \quad (57)$$

$$\langle uu + su \rangle_{++} + \langle uu + su \rangle_{-+} = \langle uu + su \rangle_{+-} + \langle uu + su \rangle_{--}, \quad (58)$$

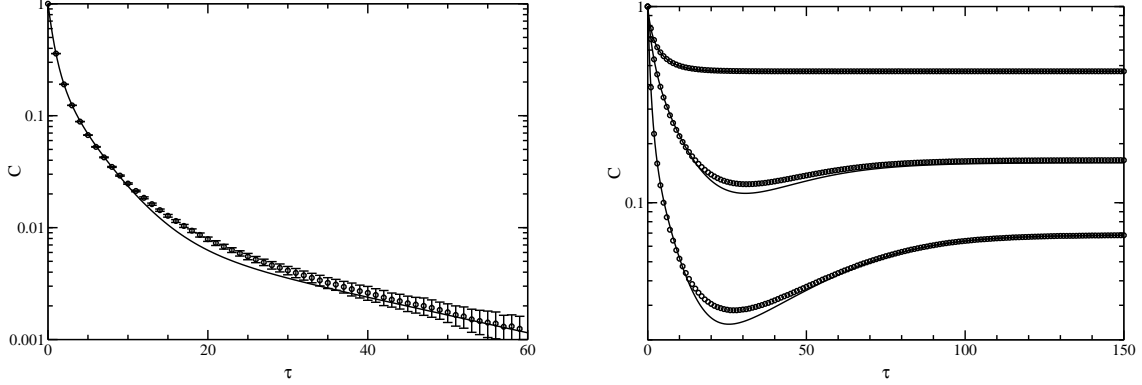


Figure 4: Two-time correlations  $C(t_1 + \tau, t_1)$  as a function of  $\tau$ , for  $K = 3$ . Solid lines: numerical integration of the differential equations, see the text for details. Symbols: Monte Carlo simulations. Left:  $\beta = 1$ ,  $t_1 = 0$ . Numerical simulations averaged on 200 samples of size  $N = 10^7$ . Right:  $\beta = 1.2$ ,  $t_1 = 0$  (bottom), 30 (middle), 150 (top). Numerical simulations averaged on 200 samples of size  $N = 3 \cdot 10^6$ , error bars are smaller than the symbol size.

Boundary conditions also constrain the value of  $q$  when  $t_1 = t_2$ . Obviously  $q_{+-} = q_{-+} = 0$  at equal times, and

$$q_{\sigma\sigma}(uu, us, su; t, t) = \delta_{us,0} \delta_{su,0} p_{\sigma}(uu; t) . \quad (59)$$

An evolution equation with respect to  $t_2$  for  $q_{\sigma_1\sigma_2}(uu, us, su; t_1, t_2)$  can be closed using factorization approximations similar to those used in Sec.3.3, here we only state the result:

$$\begin{aligned} \frac{d}{dt_2} q_{\sigma_1\sigma_2}(uu, us, su; t_1, t_2) = & \\ - q_{\sigma_1\sigma_2}(uu, us, su)W(uu + su) + q_{\sigma_1, -\sigma_2}(us, uu, ss)W(ss + us) & \\ + \frac{\langle uuW(uu + su) \rangle_{-\sigma_1 - \sigma_2}}{\langle uu \rangle_{\sigma_1\sigma_2}} [-uu q_{\sigma_1\sigma_2}(uu, us, su) + (uu + 1)q_{\sigma_1\sigma_2}(uu + 1, us - 1, su)] & \\ + \frac{\langle usW(uu + su) \rangle_{-\sigma_1\sigma_2}}{\langle us \rangle_{\sigma_1\sigma_2}} [-us q_{\sigma_1\sigma_2}(uu, us, su) + (us + 1)q_{\sigma_1\sigma_2}(uu - 1, us + 1, su)] & \\ + \frac{\langle suW(uu + su) \rangle_{\sigma_1 - \sigma_2}}{\langle su \rangle_{\sigma_1\sigma_2}} [-su q_{\sigma_1\sigma_2}(uu, us, su) + (su + 1)q_{\sigma_1\sigma_2}(uu, us, su + 1)] & \\ + \frac{\langle ssW(uu + su) \rangle_{\sigma_1\sigma_2}}{\langle ss \rangle_{\sigma_1\sigma_2}} [-ss q_{\sigma_1\sigma_2}(uu, us, su) + (ss + 1)q_{\sigma_1\sigma_2}(uu, us, su - 1)] , & \end{aligned} \quad (60)$$

where we suppressed the explicit time dependence of  $q$  in the right-hand side to lighten notations.

One can easily exploit these equations to compute the two-time correlation  $C(t_2, t_1)$  for a given initial configuration at  $t = 0$ . The first task is to determine  $p_{\sigma}(u; t_1)$  by a numerical integration of the equations (28) between  $t = 0$  and  $t = t_1$ . Using then the boundary condition (59) and the evolution equations (60), one obtains  $q$  and finally  $C$  through (56). We confront in Fig. 4 the results of such a procedure with Monte Carlo numerical experiments, which are in satisfying agreement with each other.

## 7 Connection with dynamical replica theory

### 7.1 Basic assumptions of dynamical replica theory

In this section, we are going to show the equivalence of our approximations to the dynamical replica theory (DRT) [29, 30] under the assumption of replica symmetry. To do so, we will derive

the closure equations we used in Sec. 3 starting from the assumptions of the dynamical replica approach.

Similar to our approach, DRT aims at an approximate description of the non-equilibrium dynamics of disordered systems by means of projecting the dynamics onto an array  $\vec{q}$  of  $n$  observables, and by approximately closing the corresponding equations. The method becomes exact if the following two properties are fulfilled:

- (i) The observables in  $\vec{q}$  have self-averaging properties along the dynamics, i.e. they follow their average trajectories with probability one in the thermodynamic limit.
- (ii) At each time, all microscopic configurations  $\vec{\sigma} = (\sigma_1, \dots, \sigma_N)$  having the same values of all observables in  $\vec{q}$  are equi-probable.

The first assumption is not expected to pose serious problems if, e.g., densities or fractions of vertices with certain characteristics are considered. The second assumption, on the other hand, is much more crucial: it is obviously true in thermal equilibrium if the energy density is included in  $\vec{q}$ . Indeed the probability distribution of microscopic configurations is then given by the Boltzmann-Gibbs distribution, i.e. it depends on the actual configuration only via one observable, the energy. There is, however, no reason why this should hold far from equilibrium. In fact, as discussed before, we have observed that the inclusion of more and more sophisticated observables gives a better and better description of the dynamics of the system.

At variance with the original DRT, where replicas are introduced to average over the disorder of the Sherrington-Kirkpatrick model [34], we are going to use the cavity method [7]. The latter is more efficient to average over the quenched disorder of diluted systems, in our case represented by the random regular graph on which the Ising model is defined. Even if this average is almost trivial in the case of a random regular graph, where the disorder enters only via large loops, i.e. via self-consistency conditions, this method can be easily extended to fluctuating connectivities or random interaction strengths.

## 7.2 The binomial approximation

Let us start the discussion with the binomial approximation, i.e. with the case where the dynamics is completely approximated by the behavior of the energy and the magnetization densities. The two assumptions of DRT stated above result in the following approximation,

$$\mathcal{P}(\vec{\sigma}, t) = \frac{\delta(m(t) - \frac{1}{N} \sum_i \sigma_i) \delta(e(t) - \frac{1}{N} H(\vec{\sigma}))}{\sum_{\vec{\sigma}} \delta(m(t) - \frac{1}{N} \sum_i \sigma_i) \delta(e(t) - \frac{1}{N} H(\vec{\sigma}))}. \quad (61)$$

Instead of working directly in this generalized micro-canonical framework, we use a generalized canonical approach introducing conjugate parameters for the energy, i.e. a formal inverse temperature  $\beta(e, m)$ , and for the magnetization, i.e. a formal external field  $\gamma(e, m)$ . We thus replace Eq. (61) by

$$\mathcal{P}(\vec{\sigma}, t) = \frac{1}{Z(\beta(e, m), \gamma(e, m))} \exp \left\{ -\beta(e, m) H(\vec{\sigma}) - \gamma(e, m) \sum_i \sigma_i \right\}. \quad (62)$$

Note that the formal temperature  $\beta(e, m)$  is different from the physical temperature  $\beta$ , as long as the system is not equilibrated. Both conjugate parameters have to be adjusted such that the average values of the energy and magnetization density assume the desired values  $e(t)$  and  $m(t)$ . In the thermodynamic limit, the measure becomes sharply concentrated around these values.

Using these weights for the microscopic configurations, we have to prove that Eq. (21) holds, i.e. that the two assumptions of DRT lead to the same closure of our approximate dynamical equations. This can be easily obtained using the Bethe-Peierls approach sketched in Sec. 2, the only modification is due to the additional external field. The analysis follows, however, exactly the same steps, and it leads in particular to the desired binomial closure assumption.

### 7.3 The independent-neighbor approximation

The case of the independent neighbor approximation is only slightly more involved. We have to show that the assumption that all configurations with the same  $p_\sigma(u)$  are equiprobable leads to the desired factorization of the joint distribution of neighbors, and thus to the dynamical equations of Sec. 3.3. More precisely, we demonstrate that, under the above-stated assumption, the conditional probability of finding a vertex with  $u_2$  unsatisfied edges, following a  $\sigma \rightarrow \pm\sigma$  edge from a vertex with  $u_1$  antiparallel neighbors, equals

$$\begin{aligned} p(u_2 \mid \sigma, u_1 \rightarrow \sigma) &= \frac{p_{\sigma,\sigma}(u_1, u_2)}{\sum_{u_2} p_{\sigma,\sigma}(u_1, u_2)} \propto (K - u_2) p_\sigma(u_2) , \\ p(u_2 \mid \sigma, u_1 \rightarrow -\sigma) &= \frac{p_{\sigma,-\sigma}(u_1, u_2)}{\sum_{u_2} p_{\sigma,-\sigma}(u_1, u_2)} \propto u_2 p_{-\sigma}(u_2) , \end{aligned} \quad (63)$$

and it is thus independent on  $u_1$ , cf. the closure assumptions (27).

Taking any microscopic configuration  $\vec{\sigma}$ , the distribution  $p_\sigma(u)$  is calculated as

$$p_\sigma(u) = \frac{1}{N} \sum_{i=1}^N \delta_{\sigma_i, \sigma} \delta_{u_i(\vec{\sigma}), u} , \quad (64)$$

where  $u_i(\vec{\sigma}) = \sum_j J_{ij} \delta_{\sigma_i, -\sigma_j}$  counts the number of unsatisfied links incident to  $i$ . Again, in analogy to a microcanonical calculation, we should sum over all configurations having exactly the same values of  $p_\sigma(u)$  for all  $\sigma \in \{\pm 1\}$  and  $u \in \{0, \dots, K\}$ . As in the the previous section, we can circumvent the explicite microcanonical calculation by going to a generalized canonical ensemble by introducing formal inverse temperatures  $\beta_\sigma(u)$  for every pair  $(\sigma, u)$ . These formal temperatures have to be adjusted in order to constrain the  $p_\sigma(u)$  to the desired values. Out of equilibrium, they are not directly related to the physical temperature  $\beta$ .

We consequently have to determine the partition function

$$\begin{aligned} Z &= \sum_{\{\sigma_i\}_{i=1}^N} \exp \left\{ \sum_{\sigma, u} \beta_\sigma(u) \sum_{i=1}^N \delta_{\sigma_i, \sigma} \delta_{u_i(\vec{\sigma}), u} \right\} \\ &= \sum_{\{\sigma_i\}_{i=1}^N} \exp \left\{ \sum_{i=1}^N \beta_{\sigma_i}(u_i(\vec{\sigma})) \right\} . \end{aligned} \quad (65)$$

Proceeding in close analogy with Sec. 2, we introduce partial partition functions  $Z_{i|j}(\sigma_i, u_{i|j})$  for the subtrees rooted in vertex  $i$ , with edges  $(i, j)$  removed. The values of  $\sigma_i$  and  $u_{i|j}$  are fixed, where  $u_{i|j}$  denotes the number of unsatisfied edges including vertex  $i$  but not  $j$ . Denoting the set of all neighbors of  $i$  in the subtree by  $V_{i|j}$ , the partition function can be calculated by an iterative procedure:

$$\begin{aligned} Z_{i|j}(\sigma_i, u_{i|j}) &= \sum_{I \subset V_{i|j}: |I|=u_{i|j}} \prod_{k \in I} \left[ \sum_{u_{k|i}=0}^{K-1} Z_{k|i}(-\sigma_i, u_{k|i}) \exp \{ \beta_{-\sigma_i}(u_{k|i} + 1) \} \right] \\ &\quad \prod_{k \in V_{i|j} \setminus I} \left[ \sum_{u_{k|i}=0}^{K-1} Z_{k|i}(\sigma_i, u_{k|i}) \exp \{ \beta_{\sigma_i}(u_{k|i}) \} \right] . \end{aligned} \quad (66)$$

Introducing generalized cavity fields as  $h_{i|j}(\sigma, u) = \ln \{ Z_{i|j}(\sigma, u) / Z_{i|j}(-1, K-1) \}$ , and looking for a homogeneous solution  $h_{i|j}(\sigma, u) = h(\sigma, u)$  for all edges  $(i, j)$ , we obtain the following  $2K-1$  self-consistency equations:

$$h(\sigma, u) = \ln \left\{ \binom{K-1}{u} f(\sigma, -\sigma)^u f(\sigma, \sigma)^{K-1-u} \right\} \quad (67)$$

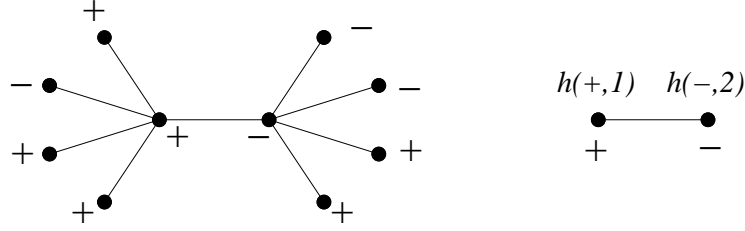


Figure 5: On the left, an example for a subgraph contributing to  $p_{+-}(2, 3)$  is given. Within the cavity calculation, the influence of the exterior part is replaced by the corresponding cavity fields  $h(+, 1)$  and  $h(-, 2)$ , cf. Eq. (70).

with

$$f(\sigma, \tau) = \frac{\sum_{u_1=0}^{K-1} e^{h(\tau, u_1) + \beta_{-\sigma}(u_1 + \delta_{\sigma, -\tau})}}{\sum_{u_1=0}^{K-1} e^{h(+, u_1) + \beta_{+}(u_1 + 1)}} . \quad (68)$$

Note that, by plugging Eq. (67) into (68), these equations can easily be reduced to only three self-consistent equations for  $f(+, +)$ ,  $f(+, -)$  and  $f(-, -)$ , whereas  $f(-, +) = 1$  by definition. Once these quantities are known, we can immediately determine the distribution

$$p_{\sigma}(u) = \binom{K}{u} f(\sigma, -\sigma)^u f(\sigma, \sigma)^{K-u} e^{\beta_{\sigma}(u)} . \quad (69)$$

As already said, the formal temperatures have to be adjusted in such a way that all  $p_{\sigma}(u)$  take the desired values.

In order to show that the independent-neighbor approximation holds in this ensemble, we have to calculate the joint distribution  $p_{\sigma_1, \sigma_2}(u_1, u_2)$  for neighboring vertices. As an example we are analyzing the case  $\sigma_1 = +1$ ,  $\sigma_2 = -1$ , the other combinations work out analogously, see Fig. 5 for an illustration:

$$p_{+-}(u_1, u_2) \propto e^{h(+, u_1-1) + h(-, u_2-1) + \beta_{+}(u_1) + \beta_{-}(u_2)} \quad (70)$$

$$\begin{aligned} &\propto \binom{K-1}{u_1-1} f(+, -)^{u_1-1} f(+, +)^{K-u_1} \binom{K-1}{u_2-1} f(-, -)^{K-u_2} e^{\beta_{+}(u_1) + \beta_{-}(u_2)} \\ &\propto u_1 p_{+}(u_1) u_2 p_{-}(u_2) f(+, -)^{-1} \end{aligned} \quad (71)$$

For the conditional probability given in Eq. (63) we thus find

$$p(u_2 \mid +, u_1 \rightarrow -) = \frac{p_{+-}(u_1, u_2)}{\sum_{u_2} p_{+-}(u_1, u_2)} \propto u_2 p_{-}(u_2) \quad (72)$$

which is exactly the independent neighbor approximation applied to close the dynamical equations in Sec. 3.3.

This derivation can be easily generalized for the link approximation scheme. We thus conclude that the presented approach is equivalent to DRT under the assumption of replica symmetry. On the other hand, focusing on finite-connectivity models makes this approach more elegant and intuitively understandable, compared to fully connected models for which the analogous equations are much more involved [30].

## 8 Conclusions and outlook

To summarize, we have studied the dynamics of the Ising ferromagnet on a Bethe lattice. This simple and, from the point of view of statics, well-analyzed model serves as an ideal testing ground

for a series of dynamical approximation schemes first introduced in the context of the analysis of stochastic local search optimization algorithms. In particular, we have obtained a detailed characterization of the critical behavior of this mean-field model.

Whereas the presented approximation schemes work very well in this simple case, there remain crucial open questions in the dynamic of disordered diluted systems, where the disorder can be present either in fluctuating vertex degrees or in randomly chosen interactions strengths.

A first interesting application of our approach would therefore be the study of disordered ferromagnets in their Griffith phase [35, 36]. This phase is characterized by an anomalously slow relaxation behavior even in the high-temperature paramagnetic regime, which results from the existence of large regions of higher than average coupling strength.

An even more challenging problem appears if frustration is included into the model, i.e. if we turn to systems displaying a low-temperature spin-glass phase. Here the connection of our approach with DRT becomes important and opens the way for the inclusion of replica symmetry breaking effects. A challenging task in this direction would be to reproduce with such a dynamical approach the subtle phenomena of cooling schedule dependence investigated numerically in [37].

Finally, we want to mention as a future direction of research the refined analysis of stochastic local search algorithms which solve (or approximate) optimization problems like 3-satisfiability or graph coloring. This includes, e.g., the analysis of the influence of greedy heuristic steps, which was out of range before [38].

**Acknowledgment:** We are very grateful to Leticia Cugliandolo, Rémi Monasson, Andrea Montanari, Andrea Pagnani, and Annette Zippelius for various interesting and helpful discussions. We also thank the ICTP Trieste and the ISI Foundation Turin for their hospitality during this work, and the Exystence Network for financial support.

## References

- [1] W. Götze, in *Liquids, Freezing and the Glass Transition*, J.P. Hansen, D. Levesque and J. Zinn-Justin eds. Les Houches Session LI, 1989, (North-Holland, Amsterdam, 1991), 287.
- [2] F. Ritort and P. Sollich, *Adv. Phys.* **52**, 219 (2003).
- [3] M. Mézard, G. Parisi and M.A. Virasoro, *Spin glass theory and beyond*, (World Scientific, Singapore, 1987).
- [4] J.P. Bouchaud, L.F. Cugliandolo, J. Kurchan, and M. Mézard, in *Spin glasses and random fields*, A.P. Young ed., (World Scientific, 1998).
- [5] L.F. Cugliandolo, in *Slow Relaxations and nonequilibrium dynamics in condensed matter*, J.L. Barrat, M. Feigelman, J. Kurchan and J. Dalibard eds. Les Houches Session LXXVII, 2002, 367.
- [6] R. Monasson, *J. Phys. A* **31** 515 (1998).
- [7] M. Mézard and G. Parisi, *Eur. Phys. J. B* **20**, 217 (2001).
- [8] S. Franz, M. Mézard, F. Ricci-Tersenghi, M. Weigt and R. Zecchina, *Europhys. Lett.* **55** 465 (2001).
- [9] G. Biroli and M. Mézard, *Phys. Rev. Lett.* **88**, 025501 (2002).
- [10] M. Weigt and A.K. Hartmann, *Europhys. Lett.* **62**, 533 (2003).
- [11] M. Pica Ciamarra, M. Tarzia, A. de Candia, and A. Coniglio, *Phys. Rev. E* **67**, 057105 (2003).
- [12] O. Rivoire, G. Biroli, O. Martin and M. Mézard, preprint [cond-mat/0307569](https://arxiv.org/abs/cond-mat/0307569).
- [13] M.A. Garey and D.S. Johnson, *Computers and Interactability: A Guide to the Theory of NP-Completeness*, (Freeman and Co., New York, 1979).

- [14] Special issue of Artif. Intell. **81** (1996).
- [15] Special issue of Theor. Comp. Sci. **265** (2001).
- [16] S. Cocco, R. Monasson, A. Montanari and G. Semerjian, preprint [cs.CC/0302003](#).
- [17] R. Monasson and R. Zecchina, Phys. Rev. Lett. **76**, 3881 (1996).
- [18] R. Monasson, R. Zecchina, S. Kirkpatrick, B. Selman, and L. Troyansky, Nature **400**, 133 (1999).
- [19] G. Biroli, R. Monasson and M. Weigt, Eur. Phys. J. B **14**, 551 (2000).
- [20] F. Ricci-Tersenghi, M. Weigt and R. Zecchina, Phys. Rev. E **63**, 026702 (2001).
- [21] M. Mézard, G. Parisi and R. Zecchina, Science **297**, 812 (2002).
- [22] R. Mulet, A. Pagnani, M. Weigt and R. Zecchina, Phys. Rev. Lett. **89**, 268701 (2002).
- [23] A. Barrat and R. Zecchina, Phys. Rev. E **59**, R1299 (1999).
- [24] A. Montanari and F. Ricci-Tersenghi, Phys. Rev. Lett. **90**, 017203 (2003).
- [25] G. Semerjian and L.F. Cugliandolo, Europhys. Lett. **61**, 247 (2003).
- [26] G. Semerjian, L.F. Cugliandolo and A. Montanari, [cond-mat/0304333](#), J. Stat. Phys. (to appear).
- [27] G. Semerjian and R. Monasson, Phys. Rev. E **67**, 066103 (2003).
- [28] W. Barthel, A.K. Hartmann, and M. Weigt Phys. Rev. E **67**, 066104 (2003).
- [29] A.C.C. Coolen and D. Sherrington, J. Phys. A **27**, 7687 (1994).
- [30] S.N. Laughton, A.C.C. Coolen, and D. Sherrington, J. Phys. A **29**, 763 (1996).
- [31] M. Molloy and B. Reed, Random Structures and Algorithms **6**, 161 (1995).
- [32] M. E. J. Newman, S. H. Strogatz, and D. J. Watts, Phys. Rev. E **64**, 026118 (2001)
- [33] Baxter, *Exactly solved models in Statistical Mechanics*, (Academic Press, London, 1982).
- [34] D. Sherrington and S. Kirkpatrick, Phys. Rev. Lett. **35**, 1792 (1975).
- [35] A.J. Bray, Phys. Rev. Lett. **59**, 586 (1987).
- [36] A.J. Bray and H. Huifang, Phys. Rev. B **40**, 6980 (1989).
- [37] A. Montanari and F. Ricci-Tersenghi, preprint [cond-mat/0401649](#).
- [38] A. Pagnani and M. Weigt, in preparation.